Published in final edited form as:
Biofabrication. 2013 December ; 5(4): . doi:10.1088/1758-5082/5/4/045003.

Customized biomimetic scaffolds created by indirect three-dimensional printing for tissue engineering

Ju-Yeon Lee[a], **Bogyu Choi**[a], **Benjamin Wu**[a,b], and **Min Lee**[a,b]

[a]Division of Advanced Prosthodontics, University of California, Los Angeles, California 90095

[b]Department of Bioengineering, University of California, Los Angeles, California 90095

Abstract

Three-dimensional printing (3DP) is a rapid prototyping (RP) technique that can create complex 3D structures by inkjet printing of a liquid binder onto powder biomaterials for tissue engineering scaffolds. Direct fabrication of scaffolds from 3DP, however, imposes a limitation on material choices by manufacturing processes. In this study, we report an indirect 3DP approach wherein a positive replica of desired shapes was printed using gelatin particles, and the final scaffold was directly produced from the printed mold. To create patient-specific scaffolds that match precisely to a patient's external contours, we integrated our indirect 3DP technique with imaging technologies and successfully created custom scaffolds mimicking human mandibular condyle using polycaprolactone (PCL) and chitosan (CH) for potential osteochondral tissue engineering. To test the ability of the technique to precisely control the internal morphology of the scaffolds, we created orthogonal interconnected channels within the scaffolds using computer-aided-design (CAD) models. Because very few biomaterials are truly osteoinductive, we modified inert 3D printed materials with bioactive apatite coating. The feasibility of these scaffolds to support cell growth was investigated using bone marrow stromal cells (BMSC). The BMSCs showed good viability in the scaffolds, and the apatite-coating further enhanced cellular spreading and proliferation. This technique may be valuable for complex scaffold fabrication.

Keywords

Three-dimensional printing; Scaffold; Tissue engineering; Gelatin; Polycaprolactone; Chitosan

1. Introduction

Fabrication of multifunctional scaffolds that meet structural, mechanical, and nutritional requirements is vital to direct three-dimensional (3D) tissue ingrowth for the repair of large, complex, multi-tissue defects. Solid freeform fabrication (SFF) technologies were employed to build objects with well-defined architectures on the macro- and micro-scales with tissue engineering applications [1–3]. Various rapid prototyping (RP) techniques were introduced such as stereolithography (SLA), selective laser sintering (SLS), fused deposition molding (FDM) and 3D Printing (3DP) [4–11]. RP techniques provide unique ways to build accurate and highly reproducible scaffolds with minimal manpower and cost requirements compared to conventional fabrication techniques with random processes. Moreover, RP techniques enable the production of patient-specific scaffolds that precisely match a patient's contours such as large regions of craniofacial or osteochondral defects in conjunction with non-invasive imaging technologies and computer-aided-design (CAD) models [6, 12–14].

Corresponding author: Min Lee, PhD, UCLA School of Dentistry, 10833 Le Conte Avenue, CHS 23-032B, Los Angeles, CA 90095-1668, Telephone: (310) 825-4420, Fax: (310) 825-6345, leemin@ucla.edu.

3DP is one of the most investigated RP techniques based on inkjet printing liquid binder to join loose powder to create complex 3D structures [9, 15–19]. Although a 3DP technique offers innovative ways to produce biomimetic structures, the current direct 3DP approach is limited by a narrow choice of materials because the conventional direct method is highly dependent on powder material properties, requiring different printing process parameters depending on each biomaterial under consideration. Moreover, the use of common synthetic biodegradable polymers is undesirable for this technique because an organic solvents binder will dissolve most commercially available drop-on-demand printhead subsystems. To address this issue, we developed indirect 3DP technique, where inverse molds of the desired shapes are printed and the final materials are then cast into the mold cavity [9, 10]. Material choice is highly flexible with this approach because many different materials can be cast under similar printing process parameters. While this approach has the capability of controlling the external shape of scaffolds with high resolution, it was undesirable for the fabrication of complex internal microstructures with overhang and undercuts. In our previous study [9], the villi-shaped scaffolds did not accurately capture the original CAD model and the villus architecture tapered toward the villus tip as measured by cross sectioned images. The reason was that viscous polymer solutions or porogen-containing scaffolding materials could not uniformly flow throughout the complex internal volume of the printed mold. Casting uniformity will be more problematic in the fabrication of scaffolds with internal undercuts such as intersecting channels.

This study reports a modified indirect 3DP protocol using a positive mold, where the final structure was produced directly from a positive replica of a desired scaffold shape. In this technique, the mold was fabricated by printing an aqueous binder onto a powder bed of gelatin porogens. The created mold was infiltrated with common biodegradable polymers and a porous polymer structure was produced by particle leaching of porogens. To demonstrate the ability of this approach to create the complex scaffolds with undercuts directly from medical imaging data, the anatomic shape of a human mandibular condyle with orthogonally interconnected internal channels was selected arbitrarily and constructed based on computed topography (CT) scan and CAD models for potential osteochondral tissue engineering for the treatment of osteoarthritis. Micro- and nano-scale features were created on the scaffold surface by adding a biomimetic apatite coating to engineer more osteoinductive scaffolds. The feasibility of the scaffolds to support cell attachment and growth was demonstrated using bone marrow stromal cells (BMSC), the most commonly used cell source for bone and cartilage tissue engineering.

2. Materials and methods

2.1 Materials

Chitosan (CH, 50–190 kDa, 75–85% deacetylated), chondroitin sulfate sodium salt (CS, MW 50,000, ≥ 60% type A) from bovine trachea, pentasodium tripolyphosphate (TPP), polycaprolactone (PCL, Mn 70,000–90,000), and chloroform, were purchased from Sigma (St. Louis, MO). Gelatin (Bloom 175) was purchased from Affymetrix (Santa Clara, CA).

2.2 Design and fabrication

The procedure for mold design and scaffold fabrication is shown in figure 1. In brief, the anatomic shape of mandibular condyle was isolated from the CT scan using commercially available software (Mimics, Materialise, Ann Arbor, MI). The defined image data were 3D rendered and converted to an STL file for 3D printing. CAD software (Solidworks, Waltham, MA) was used to create 2 mm orthogonal intersecting channels spaced 1 mm apart. The objects were sliced into 2D layers and then each individual sliced layer was built sequentially on a commercially available 3DP machine (Z402, Zcorp, Burlington, MA) as

previously described [9, 10]. Prior to printing, the gelatin powder was sieved to a range of 106 μm to 212 μm in a sieve shaker (W.S. Tyler, Mentor, OH). Polyacrylic acid (PAA, Sigma) was added to the stock water-based binder (ZB7, Zcorp) with a 1:10 volume ratio to enhance the strength of a printed mold for subsequent processing. During the fabrication, 0.229 mm layer of sieved gelatin powder was spread, and the binder was printed selectively to form the 2D pattern. The process was repeated layer by layer until the final objects were completed.

PCL scaffolds were fabricated by infiltrating the printed gelatin molds with PCL in chloroform (7% w/w). Scaffolds were dried in a fume hood, and solvent was removed by freeze-drying overnight. Molds were removed by placing them in deionized water at 50 °C for 6 hours. The gelatin-leached PCL scaffolds were collected and dried at room temperature in a fume hood overnight for further studies. For CH scaffolds fabrication, the created PCL scaffolds were infiltrated with CH solution (5% w/v) in 1 N acetic acid for 6 hours, frozen at − 80 °C for 8 hours, and lyophilized in a freeze dryer overnight. The obtained CH scaffolds were crosslinked with 5% (w/v) CS and TPP solution for 1 hour and neutralized in 1N NaOH for 20 min. The scaffolds were washed with ddH_2O, disinfected by immersing them into 70% ethanol for 30 min, and lyophilized overnight prior to further studies.

2.3 Biomimetic apatite coating

Apatite coating solution was prepared as described previously [20–22]. Briefly, simulated body fluid (SBF) was prepared by dissolving $CaCl_2$, $MgCl_2{\cdot}6H_2O$, $NaHCO_3$, and $K_2HPO_4{\cdot}3H_2O$ into ddH_2O. The pH of solution was adjusted to pH 6.0. Then, Na_2SO_4, KCl, and NaCl were added. The final pH of solution was adjusted to pH 6.5 (SBF 1). Mg^{2+} and HCO_3^- free SBF (SBF 2) was prepared by dissolving NaCl, $CaCl_2$, and $K_2HPO_4{\cdot}3H_2O$. The pH of solution was adjusted to pH 6.5. All solutions were sterile filtered through a 0.22 μm PES membrane (Nalgene, NY). The obtained scaffolds were subjected to glow discharge argon plasma etching (Harrick Scientific, Ossining, NY). The etched scaffolds were incubated in SBF 1 for 1 day and transferred to SBF 2 for another day at 37 °C. The apatite-coated scaffolds were washed with ddH_2O to remove excess ions and lyophilized prior to further studies.

2.4 Scanning electron microscopy

The morphology of scaffolds was observed by scanning electron microscopy (SEM, Nova Nano SEM 230/FEI, Hillsboro, OR). Prior to SEM analysis, the scaffolds were mounted on aluminum stubs and gold coated with a sputter coater at 20 mA under 70 mTorr for 50 s.

2.5 ATR-FTIR

The chemical structure of the scaffolds was analyzed using Attenuated Total Reflection-Fourier Transform Infrared Spectroscopy (ATR-FTIR) before and after apatite coating. The samples were placed in contact with a diamond ATR window. FTIR (Avatar 360 Thermo Nicolet spectrometer, Thermo Electron Inc., San Jose, CA) absorbance spectra from 2000 to 500 cm^{-1} wavenumbers was obtained.

2.6 Cell seeding and proliferation

Mouse bone marrow stromal cells (BMSC, ATCC, VA) were used in Dulbeccos' modified Eagles' medium (DMEM, Invitrogen) with low glucose, 10% fetal bovine serum (FBS, Invitrogen), 100 U/mL penicillin, 100 μg/mL streptomycin. Cells were trypsinized upon 80% confluence and each scaffold (7mm × 4mm × 4mm) was seeded with 50 μl of cell suspension at a concentration of 5×10^6 cells/mL. After incubation for 2 hours, the scaffolds were placed in a 24-well polystyrene plate and cultured with 1 mL of complete DMEM at 37

°C in 5% CO_2 humidified incubators up to 14 days. To observe the proliferation of BMSC, cell/scaffold constructs were washed with PBS and stained with calcein solution (Invitrogen) at 37 °C for 10 minutes. Stained samples were observed using a fluorescence microscope (Olympus, Lake Success, NY). The AlamarBlue assay kit (Invitrogen) was used to further measure the proliferation of cells on the scaffolds. The scaffolds were washed once with PBS, transferred to a new culture plate, and incubated with AlamarBlue solution for 3 hours at 37 °C. AlamarBlue fluorescence was assayed at 530 nm (excitation) and 590 nm (emission). The experiment was performed in triplicate manner.

3. Results and discussion

3.1. Scaffold fabrication

Scaffolds with complex 3D anatomic shape were fabricated by indirect 3DP technique integrated with imaging technique. Anatomic design featuring a mandibular condyle was generated from 2D images acquired from CT data (figure 2a). To test the ability of the indirect technique to precisely control internal morphology of scaffolds, orthogonal interconnected channels were created in CAD software (figure 2b). Channel design was employed in tissue engineering scaffolds to enhance the mass transport of oxygen and nutrients to maintain cell viability and facilitate vessel ingrowth within the large tissue graft [23, 24]. Figure 2c shows a fabricated gelatin mold with an external shape matching the mandibular condyle design and predefined internal architecture. Gelatin is derived from naturally occurring collagen and has been widely used for many biomedical and tissue engineering applications due to its excellent biocompatibility and biodegradability [25–28]. Furthermore, gelatin has been used as porogen to create porous scaffolds where gelatin particles were cast in a polymer solution and the gelatin porogen subsequently leached out with water [29, 30]. In addition to gelatin, we have tested various water soluble disaccharides such as sucrose, maltose, and lactose as building materials for 3DP. Although sucrose particles were able to be processed by 3DP, low build resolution was observed with a 200% increase of its original size in the CAD design at a feature size of 1000 μm. Moreover, it was difficult to remove the unbound particles trapped in channels after printing. This is likely due to the hygroscopic nature of sucrose particles and their affinity for atmospheric moisture causing particle clumping. We also tested less water soluble disaccharides such as maltose and lactose; however, the fabricated parts were not mechanically strong enough to handle these probably because the aqueous binder used did not properly wet the particle surface to be held together. Among the materials tested, gelatin was found to be the most promising for releasing the parts from a powder bed and removing entrapped powders with good handling property and mechanical stability. The wall thickness of the printed gelatin mold was approximately 1.3 mm, 300 μm larger than the designed architectures. The additional wall thickness decreased the original channel size from 2 mm to 1.7 mm in the 3DP mold. This difference may be attributed to binder spreading and subsequent incorporation of adjacent particles, reducing printing resolution. The PAA binder did not saturate the loosely packed powder bed of irregular gelatin particles and left enough free space between the printed particles for the subsequent infiltration of PCL (figure 2e).

PCL scaffolds were produced by infiltrating PCL solution into printed gelatin molds (figure 3a). PCL is a synthetic resorbable polymer extensively employed in tissue engineering applications due to its good degradable characteristics by hydrolysis and the complete absorption of degradation byproducts through metabolic pathways [31, 32]. Most synthetic biodegradable polymers used for these applications such as poly lactic acid (PLA) and poly glycolic acid (PGA), however, are not water soluble, requiring the use of organic solvents that are not compatible with current drop-on-demand print systems. Because gelatin is insoluble in most of the organic solvents which are commonly used to solubilize synthetic

biodegradable polymers, infiltration of PCL in chloroform was successfully processed in the gelatin mold. The fabricated PCL scaffolds matched well with the architectures of the gelatin molds. Furthermore, gelatin particles served as porogen, which was removed by particulate leaching in water to provide porous microarchitecture in scaffolds. High porosity and pore interconnectivity are critical for cell ingrowth and mass transport in 3D constructs. The interior morphology of the PCL scaffolds showed highly interconnected porous structures with a pore size range of 100–200 μm, which was similar to the size of the gelatin particles used (figure 3c).

Natural polymers such as polysaccharides (hyaluronic acid, CH, alginate) and proteins (collagen, gelatin, fibrin) are attractive for tissue engineering because of their biological origin and excellent biocompatibility [33, 34]. The compatibility of this technique with common natural polymers was further exploited using CH (figure 3d). CH is a naturally derived polysaccharide widely used for many pharmaceutical and biomedical applications [35–37]. The structural similarity of the CH backbone to disaccharide units of glycosaminoglycans found in the extracellular matrix (ECM) of bone and cartilage makes it more favorable for tissue regeneration [38, 39]. Fabricated CH scaffolds showed low mechanical integrity and were destroyed in post-processing.

One of the distinctive properties of CH is its cationic nature that allows the formation of stable ionic complexes with various multivalent water-soluble anionic molecules under mild physiological conditions [40–42]. Structural stability of the fabricated CH scaffolds was achieved by crosslinking with TPP and CS. The external shape of the crosslinked scaffolds was well preserved with slight distortion of channel walls.

3.2. Biomimetic apatite coating

Current 3D printing techniques are not able to produce a structure containing micro-and nano-features that can influence cell behavior in the scaffolds because of the limited resolution of this technology. Because very few biomaterials are truly inductive, we engineered inductive scaffolds by modifying inert and conductive 3D printed materials with a biomimetic nano-apatite coating for potential bone tissue engineering applications. We have previously developed biomimetic processing strategies to confer a bone mineral-mimicking apatite microenvironment to 3D scaffolds [20, 43]. After investigating the interactions of apatite with proteins and cells, we showed that the biomimetic apatite coating provided a sustained release of loaded proteins as well as enhanced overall osteoinductivity on the various biomaterial surfaces such as Poly Lactic-co-Glycolic-Acid (PLGA), CH, and tricalcium phosphate (TCP) [43–46]. Apatite coating of scaffolds was successfully achieved by incubating the printed PCL and CH scaffold in simulated body fluids. The created apatite coating exhibited plate-like morphology on the scaffolds (figure 4b and d) while non-coated scaffolds showed rather smooth surfaces (figure 4a and c).

Apatite formation on the scaffolds was further confirmed by ATR-FTIR analysis (figure 5). After incubating in SBF, the scaffolds showed unique peaks of phosphate groups (PO_4^{3-}) at 1030 cm^{-1}, 950 cm^{-1} and 470 cm^{-1} and carbonate group (CO_3^{2-}) at 1630 cm^{-1} indicating carbonate apatite formation on the scaffolds.

3.3. Cell proliferation

BMSCs were cultured on the fabricated PCL and CH scaffolds for up to 14 days to investigate the feasibility of these scaffolds supporting cell growth (figure 6a). It was observed that BMSCs remained round in shape on the PCL scaffolds and the cell density increased over a 14 day period. BMSCs cultured on the apatite-coated PCL scaffolds, however, demonstrated cellular spreading and completely covered the porous structure of

the scaffolds by 14 days. Proliferation of seeded cells on the scaffolds was further studied by the alamarBlue assay (figure 6b). AlamarBlue fluorescence increased over the culture period and the fluorescence was significantly higher in the apatite-coated PCL scaffolds, indicating that an apatite coating enhanced the cell proliferation rate. The cell proliferation from the alamarBlue assay was corroborated with observations (figure 6a) by microscopy. In contrast, BMSCs cultured on the CH scaffold exhibited extensive spreading and continued to increase in density up to 14 days. This can be attributed to the cationic nature of CH that promotes cell adhesion and proliferation as opposed to synthetic polymers. There was no significant difference in proliferation rate between non-treated and apatite-coated CH scaffolds as shown by alamarBlue findings.

4. Conclusions

In this study, we demonstrated an indirect 3DP process for the fabrication of custom scaffolds with a specific anatomic shape and optimized internal architecture by the infiltration of common biodegradable polymer solutions into gelatin porogens and a subsequent leaching technique. The created scaffolds were found to be cytocompatible and their bioactivity was further improved by post-surface treatment. Further investigations are needed to determine if the present scaffolds can induce differentiation of cells in vitro and support functional tissue regeneration in vivo. This technique provides a promising new strategy to engineer multifunctional scaffolds for the regeneration of complex damaged tissues.

Acknowledgments

This work was supported by the National Institutes of Health grants R01 AR060213 and R21 DE021819, the International Association for Dental Research, and the Academy of Osseointegration.

References

1. Leong KF, Cheah CM, Chua CK. Solid freeform fabrication of three-dimensional scaffolds for engineering replacement tissues and organs. Biomaterials. 2003; 24:2363–78. [PubMed: 12699674]
2. Yang SF, Leong KF, Du ZH, Chua CK. The design of scaffolds for use in tissue engineering. Part II. Rapid prototyping techniques. Tissue Engineering. 2002; 8:1–11. [PubMed: 11886649]
3. Hutmacher DW, Cool S. Concepts of scaffold-based tissue engineering--the rationale to use solid free-form fabrication techniques. Journal of cellular and molecular medicine. 2007; 11:654–69. [PubMed: 17760831]
4. Fisher JP, Vehof JWM, Dean D, van der Waerden JPCM, Holland TA, Mikos AG, Jansen JA. Soft and hard tissue response to photocrosslinked poly(propylene fumarate) scaffolds in a rabbit model. Journal of Biomedical Materials Research. 2002; 59:547–56. [PubMed: 11774313]
5. Leong KF, Phua KKS, Chua CK, Du ZH, Teo KOM. Fabrication of porous polymeric matrix drug delivery devices using the selective laser sintering technique. Proceedings of the Institution of Mechanical Engineers Part H-Journal of Engineering in Medicine. 2001; 215:191–201.
6. Schek RM, Taboas JM, Hollister SJ, Krebsbach PH. Tissue engineering osteochondral implants for temporomandibular joint repair. Orthod Craniofac Res. 2005; 8:313–9. [PubMed: 16238612]
7. Zein I, Hutmacher DW, Tan KC, Teoh SH. Fused deposition modeling of novel scaffold architectures for tissue engineering applications. Biomaterials. 2002; 23:1169–85. [PubMed: 11791921]
8. Wu BM, Borland SW, Giordano RA, Cima LG, Sachs EM, Cima MJ. Solid free-form fabrication of drug delivery devices. Journal of Controlled Release. 1996; 40:77–87.
9. Lee M, Dunn JCY, Wu BM. Scaffold fabrication by indirect three-dimensional printing. Biomaterials. 2005; 26:4281–9. [PubMed: 15683652]

10. Lee M, Wu BM, Dunn JCY. Effect of scaffold architecture and pore size on smooth muscle cell growth. Journal of Biomedical Materials Research Part A. 2008; 87A:1010–6. [PubMed: 18257081]
11. Seitz H, Rieder W, Irsen S, Leukers B, Tille C. Three-dimensional printing of porous ceramic scaffolds for bone tissue engineering. Journal of Biomedical Materials Research Part B-Applied Biomaterials. 2005; 74B:782–8.
12. Colin A, Boire JY. A novel tool for rapid prototyping and development of simple 3D medical image processing applications on PCs. Computer Methods and Programs in Biomedicine. 1997; 53:87–92. [PubMed: 9186045]
13. Winder J, Cooke RS, Gray J, Fannin T, Fegan T. Medical rapid prototyping and 3D CT in the manufacture of custom made cranial titanium plates. Journal of Medical Engineering & Technology. 1999; 23:26–8. [PubMed: 10202700]
14. Eppley BL, Kilgo M, Coleman JJ 3rd. Cranial reconstruction with computer-generated hard-tissue replacement patient-matched implants: indications, surgical technique, and long-term follow-up. Plastic and reconstructive surgery. 2002; 109:864–71. [PubMed: 11884798]
15. Cima, LG.; Sachs, E.; Cima, LG.; Yoo, J.; Khanuja, S.; Borland, SW.; Wu, BM.; Giordano, RA. Computer-derived microstructure by 3D Printing: Bio- and Structural Materials. Proceedings of the SFF Symposium; 1994. p. 41-54.
16. Lam CXF, Mo XM, Teoh SH, Hutmacher DW. Scaffold development using 3D printing with a starch-based polymer. Materials Science & Engineering C-Biomimetic and Supramolecular Systems. 2002; 20:49–56.
17. Wu BM, Cima MJ. Effects of solvent-particle interaction kinetics on microstructure formation during three-dimensional printing. Polymer Engineering and Science. 1999; 39:249–60.
18. Zeltinger J, Sherwood JK, Graham DA, Mueller R, Griffith LG. Effect of pore size and void fraction on cellular adhesion, proliferation, and matrix deposition. Tissue Engineering. 2001; 7:557–72. [PubMed: 11694190]
19. Sherwood JK, Riley SL, Palazzolo R, Brown SC, Monkhouse DC, Coates M, Griffith LG, Landeen LK, Ratcliffe A. A three-dimensional osteochondral composite scaffold for articular cartilage repair. Biomaterials. 2002; 23:4739–51. [PubMed: 12361612]
20. Chou YF, Dunn JCY, Wu BM. In vitro response of MC3T3-E1 preosteoblasts within three-dimensional apatite-coated PLGA scaffolds. Journal of Biomedical Materials Research Part B-Applied Biomaterials. 2005; 75B:81–90.
21. Lee M, Li WM, Siu RK, Whang J, Zhang XL, Soo C, Ting K, Wu BM. Biomimetic apatite-coated alginate/chitosan microparticles as osteogenic protein carriers. Biomaterials. 2009; 30:6094–101. [PubMed: 19674782]
22. Chou YF, Chiou WA, Xu YH, Dunn JCY, Wu BM. The effect of pH on the structural evolution of accelerated biomimetic apatite. Biomaterials. 2004; 25:5323–31. [PubMed: 15110483]
23. Nazhat SN, Abou Neel EA, Kidane A, Ahmed I, Hope C, Kershaw M, Lee PD, Stride E, Saffari N, Knowles JC, Brown RA. Controlled microchannelling in dense collagen scaffolds by soluble phosphate glass fibers. Biomacromolecules. 2007; 8:543–51. [PubMed: 17291078]
24. Radisic M, Park H, Gerecht S, Cannizzaro C, Langer R, Vunjak-Novakovic G. Biomimetic approach to cardiac tissue engineering. Philos T R Soc B. 2007; 362:1357–68.
25. Young S, Wong M, Tabata Y, Mikos AG. Gelatin as a delivery vehicle for the controlled release of bioactive molecules. Journal of controlled release : official journal of the Controlled Release Society. 2005; 109:256–74. [PubMed: 16266768]
26. Miyoshi M, Kawazoe T, Igawa HH, Tabata Y, Ikada Y, Suzuki S. Effects of bFGF incorporated into a gelatin sheet on wound healing. Journal of biomaterials science. Polymer edition. 2005; 16:893–907. [PubMed: 16128295]
27. Sakai S, Hirose K, Taguchi K, Ogushi Y, Kawakami K. An injectable, in situ enzymatically gellable, gelatin derivative for drug delivery and tissue engineering. Biomaterials. 2009; 30:3371–7. [PubMed: 19345991]
28. Karim AA, Bhat R. Gelatin alternatives for the food industry: recent developments, challenges and prospects. Trends Food Sci Tech. 2008; 19:644–56.

29. Gong Y, Ma Z, Zhou Q, Li J, Gao C, Shen J. Poly(lactic acid) scaffold fabricated by gelatin particle leaching has good biocompatibility for chondrogenesis. Journal of biomaterials science. Polymer edition. 2008; 19:207–21. [PubMed: 18237493]
30. Draghi L, Resta S, Pirozzolo MG, Tanzi MC. Microspheres leaching for scaffold porosity control. J Mater Sci-Mater M. 2005; 16:1093–7. [PubMed: 16362206]
31. Dash TK, Konkimalla VB. Polycaprolactone based formulations for drug delivery and tissue engineering: A review. J Control Release. 2012; 158:15–33. [PubMed: 21963774]
32. Woodruff MA, Hutmacher DW. The return of a forgotten polymer-Polycaprolactone in the 21st century. Prog Polym Sci. 2010; 35:1217–56.
33. Mano JF, Silva GA, Azevedo HS, Malafaya PB, Sousa RA, Silva SS, Boesel LF, Oliveira JM, Santos TC, Marques AP, Neves NM, Reis RL. Natural origin biodegradable systems in tissue engineering and regenerative medicine: present status and some moving trends. J R Soc Interface. 2007; 4:999–1030. [PubMed: 17412675]
34. Huang S, Fu XB. Naturally derived materials-based cell and drug delivery systems in skin regeneration. J Control Release. 2010; 142:149–59. [PubMed: 19850093]
35. Kato Y, Onishi H, Machida Y. Application of chitin and chitosan derivatives in the pharmaceutical field. Curr Pharm Biotechnol. 2003; 4:303–9. [PubMed: 14529420]
36. Lee KY, Ha WS, Park WH. Blood compatibility and biodegradability of partially N-acylated chitosan derivatives. Biomaterials. 1995; 16:1211–6. [PubMed: 8589189]
37. Dodane V, Vilivalam VD. Pharmaceutical applications of chitosan. Pharmaceutical Science & Technology Today. 1998; 1:246–53.
38. Suh JKF, Matthew HWT. Application of chitosan-based polysaccharide biomaterials in cartilage tissue engineering: a review. Biomaterials. 2000; 21:2589–98. [PubMed: 11071608]
39. Lee JY, Nam SH, Im SY, Park YJ, Lee YM, Seol YJ, Chung CP, Lee SJ. Enhanced bone formation by controlled growth factor delivery from chitosan-based biomaterials. Journal of Controlled Release. 2002; 78:187–97. [PubMed: 11772460]
40. Aminabhavi TM, Agnihotri SA, Mallikarjuna NN. Recent advances on chitosan-based micro- and nanoparticles in drug delivery. J Control Release. 2004; 100:5–28. [PubMed: 15491807]
41. Zhang MQ, Bhattarai N, Gunn J. Chitosan-based hydrogels for controlled, localized drug delivery. Advanced Drug Delivery Reviews. 2010; 62:83–99. [PubMed: 19799949]
42. Bakos D, Vodna L, Bubenikova S. Chitosan based hydrogel microspheres as drug carriers. Macromolecular Bioscience. 2007; 7:629–34. [PubMed: 17477445]
43. Park H, Choi B, Nguyen J, Fan J, Sharfi S, Klokkevold P, Lee M. Anionic carbohydrate-containing chitosan scaffolds for bone regeneration. Carbohyd Polym. 2013; 97:587–96.
44. Hou Y, Hu J, Park H, Lee M. Chitosan-based nanoparticles as a sustained protein release carrier for tissue engineering applications. Journal of biomedical materials research. Part A. 2012; 100:939–47. [PubMed: 22275184]
45. Lee M, Li W, Siu RK, Whang J, Zhang X, Soo C, Ting K, Wu BM. Biomimetic apatite-coated alginate/chitosan microparticles as osteogenic protein carriers. Biomaterials. 2009; 30:6094–101. [PubMed: 19674782]
46. Hu J, Hou Y, Park H, Lee M. Beta-tricalcium phosphate particles as a controlled release carrier of osteogenic proteins for bone tissue engineering. Journal of biomedical materials research. Part A. 2012; 100:1680–6. [PubMed: 22447727]

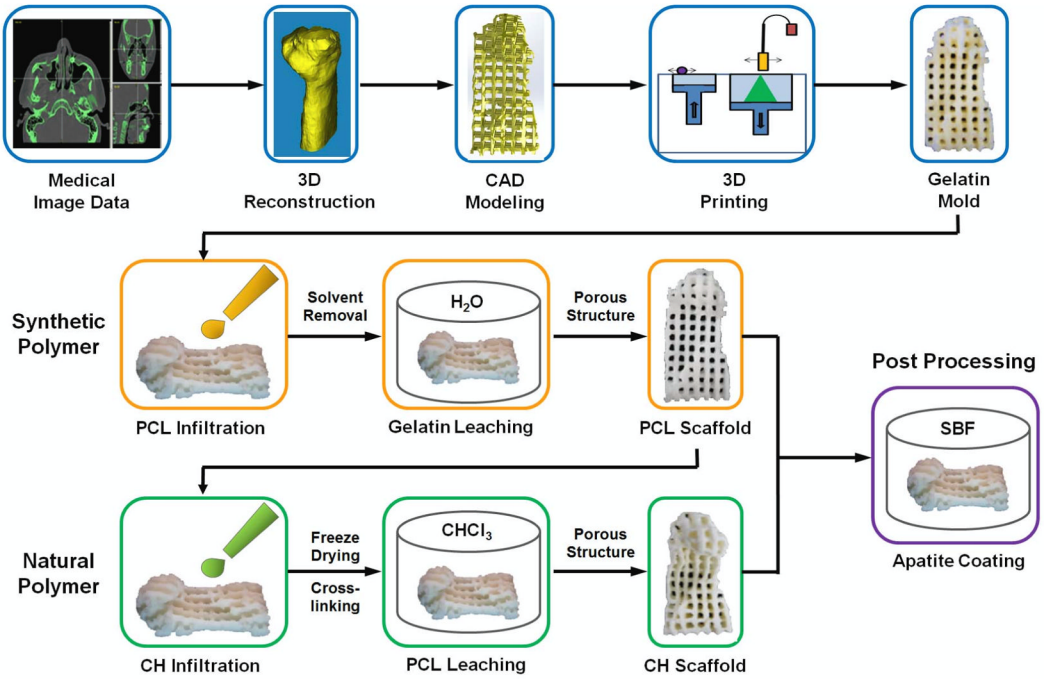

Figure 1.
Scaffold fabrication process by indirect 3DP.

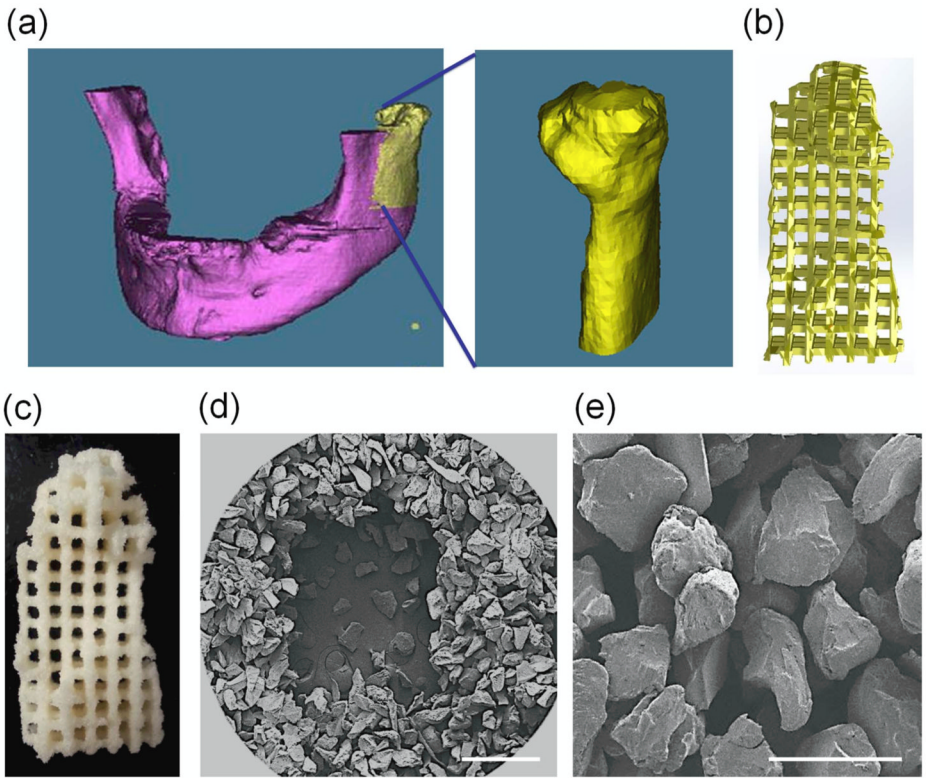

Figure 2.
(a) 3D Reconstruction of human mandible from CT images. (b) Creating of microchannels using CAD modeling. (c) 3D printed gelatin mold. SEM images of printed gelatin mold at low (d; Scale Bar = 1 mm) and high (e; Scale Bar = 200 μm) magnification.

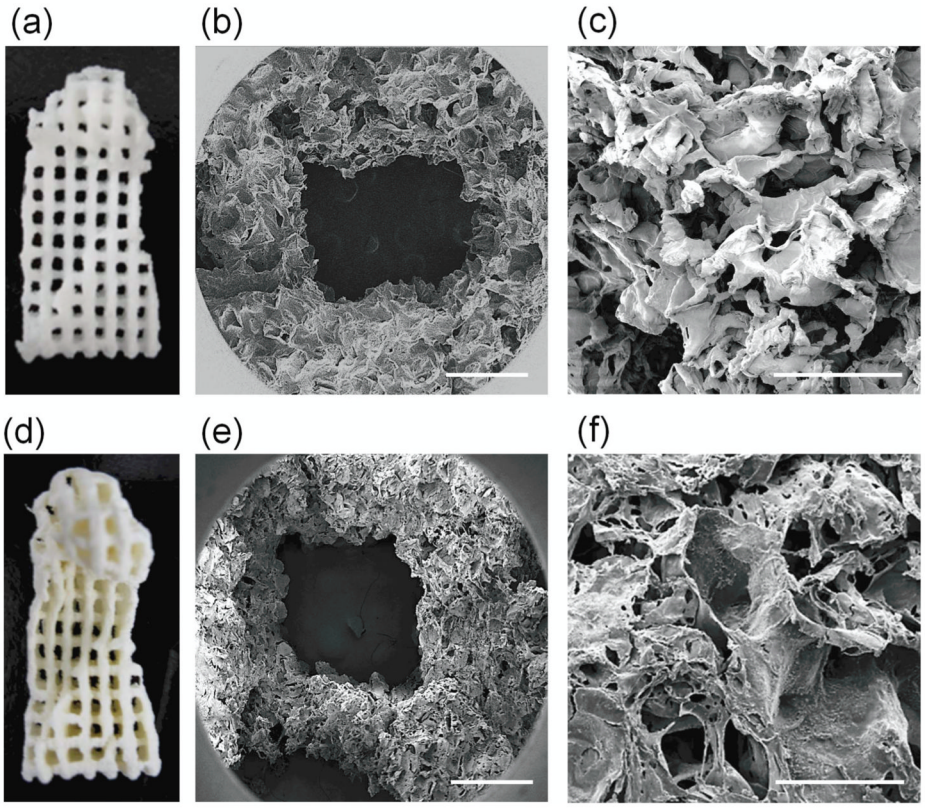

Figure 3.
PCL (a, b, c) and CH (d, e, f) scaffolds fabricated using indirect 3DP. SEM images of PCL (b, c) and CH (e, f) scaffolds at low (b, e; Scale Bar = 1 mm) and high (c, f; Scale Bar = 200 μm) magnification.

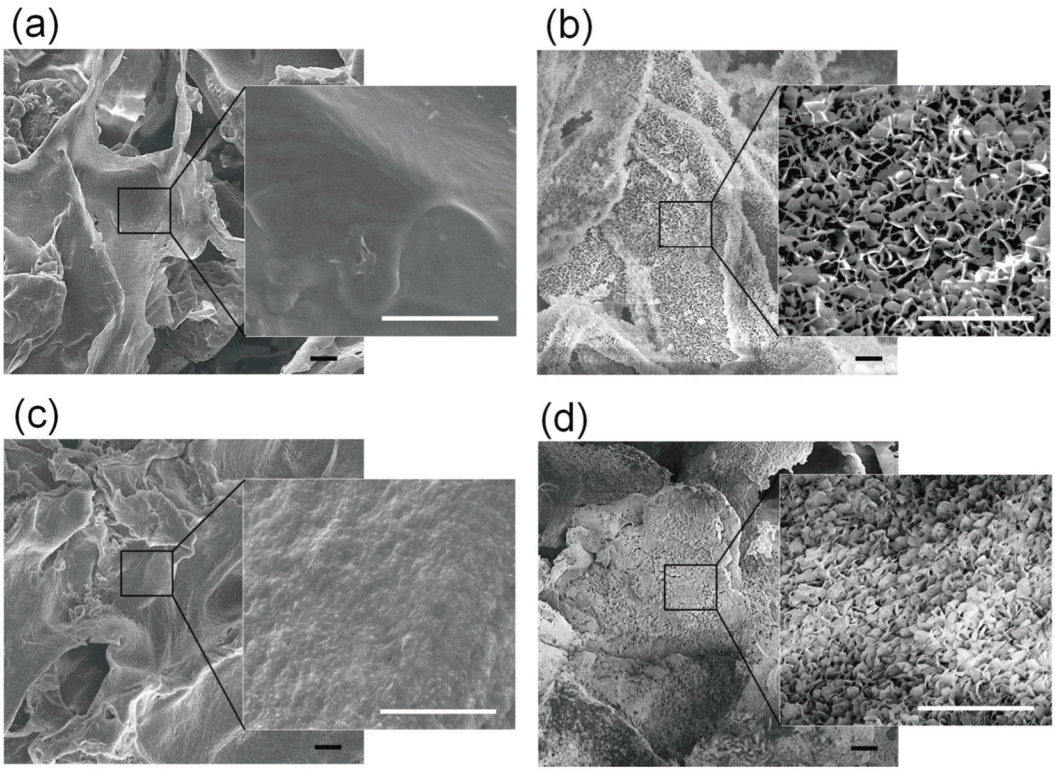

Figure 4.
SEM images of PCL (a, b) and CH (c, d) scaffolds before (a, c) and after (b, d) apatite coating. A plate-like apatite structure was formed on the surface of scaffolds after apatite coating. Scale Bar = 10 μm.

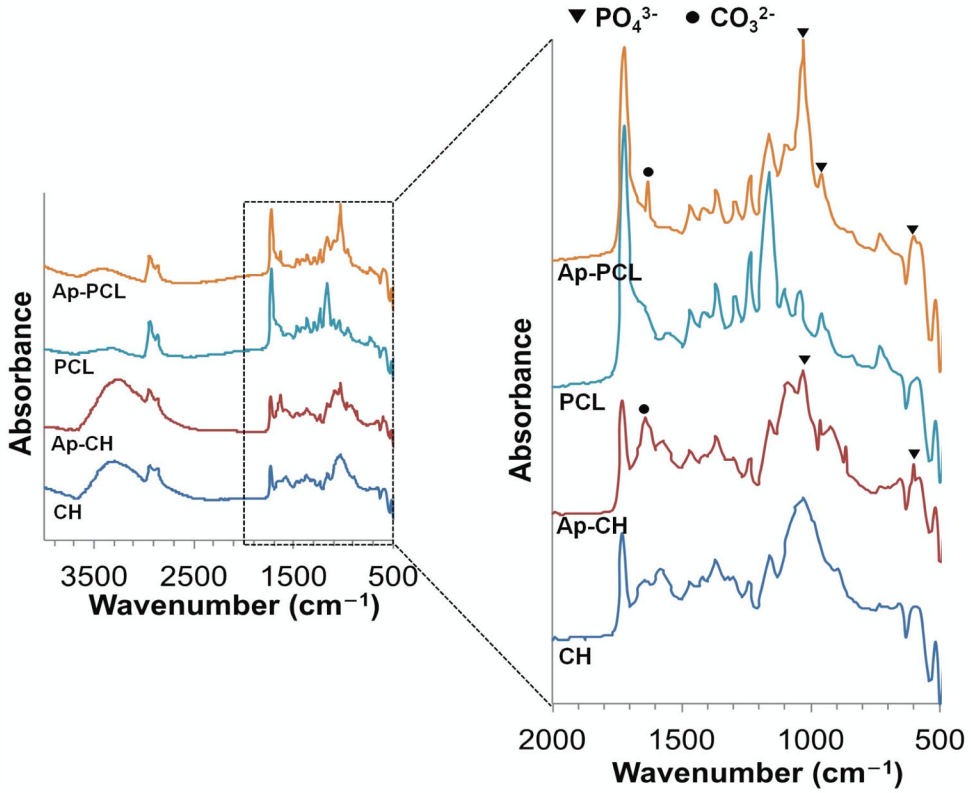

Figure 5.
ATR-FTIR Spectra of PCL and CH scaffolds before (PCL, CH) and after (Ap-PCL, Ap-CH) apatite coating. After immersing in SBF, scaffolds exhibited the characteristic peaks of phosphate (▼) and carbonate (●) groups.

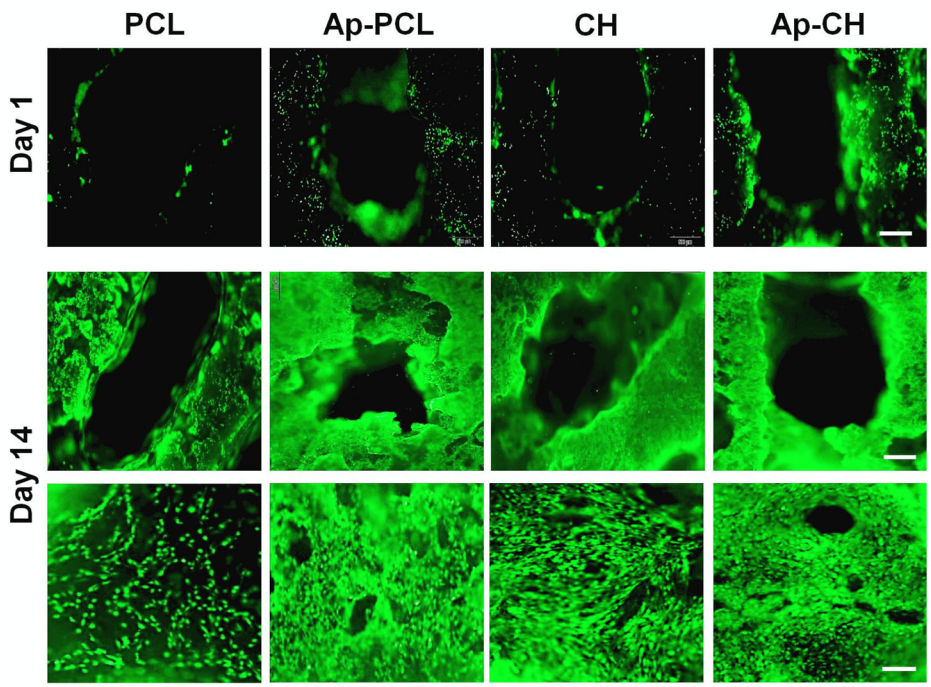

Figure 6.

Fluorescent staining of BMSCs seeded on non-coated (PCL, CH) and apatite coated (Ap-PCL, Ap-CH) scaffolds after 1 day (Scale bar = 500 μm) and 14 days (upper panel: low magnification. Scale bar = 500 μm; lower panel: high magnification. Scale bar = 100 μm) in culture.

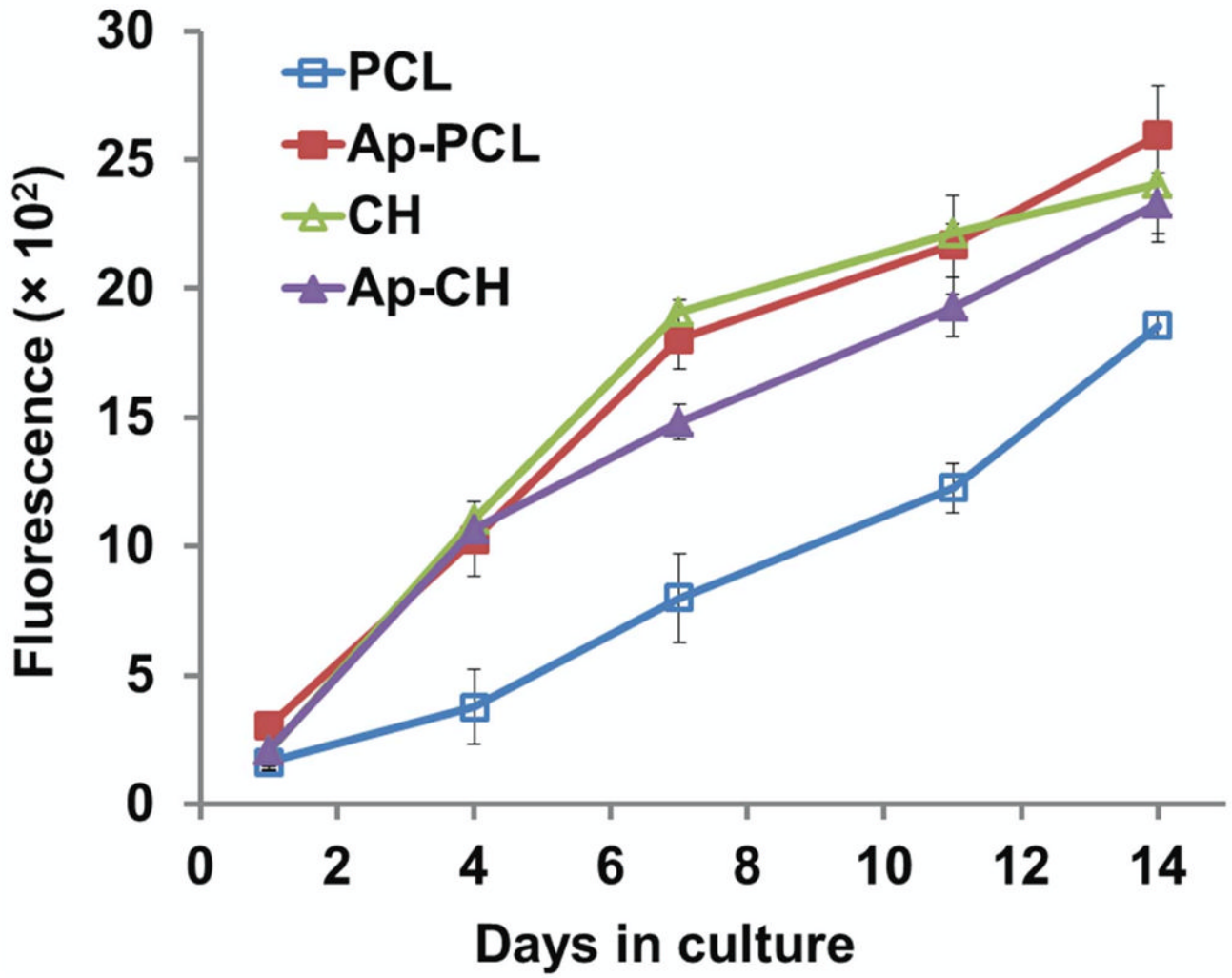

Figure 7.
AlamarBlue assay showing proliferation of BMSCs cultured on non-coated (PCL, CH) and apatite-coated (Ap-PCL, Ap-CH) scaffolds for 14 days.